Published in final edited form as:

Appl Opt. 2016 July 20; 55(21): 5479–5487. doi:10.1364/AO.55.005479.

Differentiation of tumor vasculature heterogeneity levels in small animals based on total hemoglobin concentration using magnetic resonance-guided diffuse optical tomography *in vivo*

TIFFANY C. KWONG[1], **MITCHELL HSING**[1,2], **YUTING LIN**[1,3], **DAVID THAYER**[1,4], **MEHMET BURCIN UNLU**[5], **MIN-YING SU**[1], **GULTEKIN GULSEN**[1,*]

[1]Tu and Yuen Center for Functional Onco-Imaging, Department of Radiological Sciences, University of California, Irvine, California 92697, USA

[2]Department of Electrical and Electronic Engineering, Massachusetts Institute of Technology, Cambridge, Massachusetts 02139, USA

[3]Department of Radiation Oncology, Massachusetts General Hospital and Harvard Medical School, Boston, Massachusetts 02144, USA

[4]Mallinckrodt Institute of Radiology, Washington University School of Medicine in St. Louis, St. Louis, Missouri 63110, USA

[5]Department of Physics, Bogazici University, Istanbul, Turkey

Abstract

Insight into the vasculature of the tumor in small animals has the potential to impact many areas of cancer research. The heterogeneity of the vasculature of a tumor is directly related to tumor stage and disease progression. In this small scale animal study, we investigated the feasibility of differentiating tumors with different levels of vasculature heterogeneity *in vivo* using a previously developed hybrid magnetic resonance imaging (MRI) and diffuse optical tomography (DOT) system for small animal imaging. Cross-sectional total hemoglobin concentration maps of 10 Fisher rats bearing R3230 breast tumors are reconstructed using multiwavelength DOT measurements both with and without magnetic resonance (MR) structural *a priori* information. Simultaneously acquired MR *structural* images are used to guide and constrain the DOT reconstruction, while dynamic contrast-enhanced MR *functional* images are used as the gold standard to classify the vasculature of the tumor into two types: high versus low heterogeneity. These preliminary results show that the stand-alone DOT is unable to differentiate tumors with low and high vascular heterogeneity without structural *a priori* information provided by a high resolution imaging modality. The mean total hemoglobin concentrations comparing the vasculature of the tumors with low and high heterogeneity are significant (p-value 0.02) only when MR structural *a priori* information is utilized.

*Corresponding author: ggulsen@uci.edu.

Keywords

(170.3880) Medical and biological imaging; (170.1470) Blood or tissue constituent monitoring; (170.6960) Tomography; (170.6935) Tissue characterization; (170.0110) Imaging systems; (110.4190) Multiple imaging

1. INTRODUCTION

Tumor vasculature is drastically different from normal tissue, affecting all aspects of cancer from the diagnosing and staging of a tumor, to the treatment planning and therapeutic response [1]. Dynamic contrast-enhanced magnetic resonance imaging (DCE-MRI) can noninvasively provide information on tumor vasculature such as blood perfusion and vessel permeability, with the use of an exogenous contrast agent *in vivo* [2,3].Indeed, inconsistencies in the distribution of the agent uptake in the tumor provide direct insight of the heterogeneity of the tumor vasculature, and has been reported to be biologically and diagnostically significant [4,5]. For example, studies have shown that the contrast agent uptake heterogeneity is highly correlated to the microvessel density (MVD) and the vascular endothelial growth factor (VEGF), which are both biomarkers for neoangiogenesis and have implications for drug delivery and targeted therapy [6]. The heterogeneity of the contrast agent uptake in the tumor can also provide information on cell viability and tumor stage, impacting treatment strategies [7]. For ex-ample, necrotic regions can be seen as unenhanced regions in the DCE-MRI enhancement maps. As necrotic regions are often surrounded by a thin layer of hypoxic cells, this presents some therapeutic challenges as the lack of oxygen makes these cells resistant to radiation therapy and some forms of chemotherapy [7,8]. In fact, using the DCE-MRI it has shown that quantifying the tumor contrast enhancement heterogeneity is not only useful as a measurement for treatment response, but also has the potential as a predictor of patient therapeutic outcome in many cancers including cervix, ovary, liver, and breast [3,6,9,10]. Consequently, quantifying the heterogeneity of tumor vasculature *in vivo* is important.

Currently, DCE-MRI is the gold standard for measuring tumor vascular heterogeneity *in vivo*; however, diffuse optical tomography (DOT) shows promise. DOT is a safe and in-expensive imaging modality that has great potential for cancer imaging. DOT uses near-infrared light to probe tissue properties based on endogenous contrast, and can derive functional information such as total hemoglobin concentration (HbT) and oxygen saturation. HbT can provide much needed insight on tissue metabolism and tumor malignancy [11]. For example, malignant tumors have been shown to have a higher HbT than benign tumors [12,13]. DOT can provide information on the tumor microenvironment as changes in the hemoglobin and oxygen content is directly related to the angiogenesis, metabolism, and hypoxia in the tumor [14]. Studies have shown that the HbT in the tumor is directly related to the tumor angiogenesis [15]. The oxygen saturation of the tumor can also provide valuable information on the tumor metabolism and hypoxia [16]. Such information could impact treatment strategies by helping clinicians provide personalized patient treatment. For example, a decrease in the tumor hemoglobin and oxygen content following a chemotherapy treatment has been associated with a better treatment response and outcome [17,18]. In

addition, studies have shown that the tumor metabolic response can predate anatomical changes, such as the size obtained from traditional imaging modalities during neoadjuvant chemotherapy, making DOT a promising imaging modality to monitor the early treatment response [19].

Despite its high sensitivity, DOT renders images at a low spatial resolution due to the high scattering of light in tissue. Tumor background contrast can be enhanced through external stimulation, such as gas inhalation and contrast agent injection, to improve the image quality [20,21]. However, stand-alone diffuse optical imaging systems still suffer from degraded spatial resolution and low quantitative accuracy [22,23]. To overcome this limitation, extensive effort has been spent to develop multimodality techniques that combine DOT with higher resolution imaging modalities, such as MRI, x ray, and ultrasound [21,24–26]. With this approach, the anatomical imaging modality can provide structural *a priori* information such as the tumor boundary, which can be used to guide and constrain the reconstruction algorithm by dividing the medium into tumor and background regions. It can also be used to classify different tissue types in the background (e.g., adipose and fibroglandular tissue in the breast) to assign corresponding optical properties. This multimodality approach has successfully been used to overcome the optical resolution limit of DOT for a number of applications such as determining tumor malignancy and monitoring tumor metabolic response to therapy [17,27,28].

While multimodality DOT has been largely used in human studies, there is a lack of multimodality small animal DOT systems for preclinical research [17]. As the optical properties are very heterogeneous in small animals, most preclinical multimodality imaging systems utilize fluorescent contrast for increased sensitivity and signal separation from background noise. Many studies have demonstrated that integrating structural a priori information derived from a high resolution anatomical imaging modality such as computed tomography (CT) and MRI can improve the resolution and quantitative accuracy of the recovered fluorescent source in bioluminescent (BLT) and fluorescent tomography (FT) [29–33]. In fact, functional *a priori* information derived from DOT has also been shown to improve image performance by estimating optical scattering and absorption coefficients [34,35]. In addition to improving the reconstruction by providing *a priori* information, integration with anatomical imaging modalities or non-traditional functional imaging modalities such as positron emission tomography (PET) and single-photon emission computed tomography (SPECT) can also provide a much needed cross-validation of the optical information [36–41]. Although DOT lacks the sensitivity of FT or BLT, it is much simpler to perform experimentally and computationally, has a higher signal-to-noise ratio (SNR) in detected signals, and does not require administered contrast agents. This can add an additional variable to consider for longitudinal studies, and increase the time during and in between imaging sessions [24,42]. With the growing number of cancer therapy drugs, specifically anti-angiogenic drugs that inhibit tumor growth, there is a need for small animal imaging systems to detect tumor microenvironment changes in pharmaceutical research for drug development and the study of hemodynamics. Indeed, with the progress of transgenic manipulation of small animals, there is no denying the key role animal models play in biomedical research to study disease and biological processes [24,43].

Previously, we reported on using dynamic contrast-enhanced diffuse optical tomography (DCE-DOT) with the exogenous contrast agent indocyanine green (ICG) to differentiate necrotic and viable tumors in small animals [21]. In this paper, we studied whether the HbT recovered from the stand-alone DOT and MRI structural *a priori* guided DOT is sufficient to differentiate between high and low vascular heterogeneity levels of the tumors at various stages of growth (<2.5 cm) without the use of an exogenous contrast agent for small animals. Although the tumor heterogeneous hemoglobin distribution in large necrotic tumors (≥2.5 cm) has been reported using an ultrasound (US)-guided DOT in human breast cancer, there has been a lack of DOT systems to measure the heterogeneity of tumor vasculature *in vivo* for animals [44].

In this small scale animal study, we investigated the performance of our previously developed hybrid MRI-DOT system to differentiate between tumors with low and high vasculature heterogeneity *in vivo*. To the best of our knowledge, this is the first application of MRI-DOT to characterize the heterogeneity of the vasculature of a tumor in small animals. Both the anatomical magnetic resonance (MR) and DOT measurements were simultaneously acquired utilizing a custom built hybrid MRI-DOT system that allows accurate co-registration between the MRI and optical data in time and space. These results were compared to the DCE-MRI which was used as the gold standard and taken on the same system immediately following the DOT acquisition to provide the highest degree of correlation and accuracy.

2. METHODS

A. Instrumentation

The animal experiments were performed on a previously developed small animal frequency domain DOT system that is fully integrated with MRI to acquire information simultaneously [45]. The DOT imaging interface consisted of a circular array of eight sources and eight detectors equally spaced in a radial geometry as shown in Fig. 1(c) for a total of 64 amplitude and 64 phase measurements. The temporal resolution for all 128 measurements was 16 s. This system operated at 100 MHz and used five different laser diodes with wavelengths of 665, 760, 785, 808, and 820 nm. The MRI data was taken using a 4T magnet. This hybrid system used a custom designed bird-cage type radio frequency (RF) coil integrated with the DOT interface. The MR imaging parameters were: 180 ms repetition time, 15 ms echo time, 90 deg flip-angle, 120 mm field of view, 4 mm slice-thickness, and a matrix size of 128 × 128.

B. Animal Studies

All animal procedures were approved by the Institutional Animal Care and Use Committee at the University of California, Irvine. For this study, R3230 adenocarcinoma breast tumor cells were subcutaneously implanted in Fisher rats. Ten rats were used in this study and measured at various stages of growth with 5 mm as the minimum tumor size prior to imaging. The animals were divided into two equal groups of low and high vascular heterogeneity based on tumor size and DCE-MRI. The animals were characterized using DCE-MRI data to study the enhancement heterogeneity of the tumor from a bolus

gadolinium (Gd-DTPA) tail-vein injection. We used the enhancement fraction, E_F, which is a simple method used by a number of research groups to measure tumor contrast agent enhancement heterogeneity by comparing the number of "enhanced" tumor voxels to the total tumor voxels [7,9,46]. This fraction was employed to assess the level of tumor perfusion and vasculature heterogeneity. Five out of the ten rats had a high E_F (mean 0.94 ± 0.03) and were classified as high perfusion and low heterogeneity compared to the second group with a low mean E_F score of 0.66 ± 0.09.

C. Data Analysis

For image-guided DOT, spatial information obtained by an anatomical imaging modality was used to provide information about the structural characteristics of the tumor (i.e., size, shape, location) with high resolution. This structural *a priori* data is then incorporated into the reconstruction program and has been shown to significantly improve the quantitative accuracy of DOT [45,47]. Multi-wavelength DOT and structural MR (T1 and T2 weighted) images were acquired concurrently, providing accurate co-registration between the MRI and optical data in time and space. DCE-MRI images were subsequently acquired to track the kinetics of Gd-DTPA and used as a gold standard to differentiate tumors with high and low vascular heterogeneity. The in vivo optical data was then analyzed and the cross-sectional HbT maps of the animals were reconstructed from multi-wavelength DOT measurements both with and without MR structural *a priori* information. The mean HbT was averaged over the tumor and muscle region of interest (ROI) as defined by the T1-weighted MRI.

1. Image Reconstruction—The diffusion equation was used to model the light propagation in tissue [48]:

$$\nabla \cdot [D(r)\nabla \Phi(r,\omega)] - \left[\mu_a(r) + \frac{i\omega}{c_n}\right]\Phi_x(r,\omega) = -q_0(r,\omega), \quad (1)$$

where $\Phi(r,\omega)\left(\mathrm{W}\cdot\mathrm{mm}^{-2}\right)$ is the photon density, $q_0(r,\omega)$ is an isotropic light source, $\mu_a\left(\mathrm{mm}^{-1}\right)$ is the absorption coefficient, and c_n is the speed of light corrected for the refractive index of the medium. The diffusion coefficient $D(r)$ is directly related to absorption and scattering by the following equation: $D = 1/3\left(\mu_a + \mu'_s\right)$. Additionally, to relate the fluence rate to the optical flux at the boundary, the following Robin boundary condition was used to constrain the solutions to the diffusion equation:

$$\Phi(r,\omega) + 2AD(r)\cdot\frac{\partial\Phi(r,\omega)}{\partial n} = 0, \quad (2)$$

where n is the refractive index of the medium, and A is the boundary mismatch parameter. A finite element method (FEM) based numerical solver was implemented to solve the diffusion equation. A FEM mesh was generated for each animal from the T1 weighted MR images. The size of each mesh varies for each animal. Rat 7, which is shown in the top row of Fig. 3, has 1168 and 313 nodes for the fine and coarse mesh, respectively. A dual mesh method was used to reduce computational time. A fine mesh is used to solve the forward problem, and a coarse mesh was used for the inverse problem. This inverse problem was solved by

minimizing the difference between the measured and calculated measurements. The solution can be written as

$$\Delta\mu_a = \left(J^T J + I\right)^{-1} J^T \left(\Phi_m - \Phi_c\right), \tag{3}$$

where Φ_m is the measurement. Φ_c is the flux on the measured point calculated by the forward solver from the spatial distribution of μ_a. The Jacobian matrix J was calculated with the adjoint method [49]. A Levenberg–Marquardt nonlinear optimization algorithm was used for the reconstruction process. When anatomical a priori from the MRI was available, the animal was divided into two regions, tumor and background. A "*soft a priori*" approach was performed by applying a Laplacian-type regularization method, which loosely groups the nodes in a specified region, to find the reconstructed absorption coefficient map of the animal [47]. The matrix that relates each nodal property to all other nodes is defined as the L-matrix and can be written as

$$L_{ij} = \begin{cases} 0 & \text{if } i \text{ and } j \text{ are not in the same region} \\ 1/N_r & \text{if } i \text{ and } j \text{ are in the same region} \\ 1 & \text{if } i = j \end{cases}, \tag{4}$$

where N_r represents the number of nodes included in one region. Then, the updated equation can be expressed as

$$\Delta\mu_a = \left(J^T J + L^T L\right)^{-1} J^T \left(\Phi_m - \Phi_c\right). \tag{5}$$

The algorithm is automatically stopped when the change in the residual between the forward problem and the measurements is less than 1% between successive iterations. All the reconstruction parameters, including the initial guess, damping factor, and stopping criteria, were kept the same for all the cases to ensure that there was no bias in the results. Chromophore concentration maps were obtained using the μ_a maps reconstructed at multiple wavelengths. More details on image coregistration and mesh generation were previously published [50].

2. Statistical Analysis—A two-sample Student t-test was used to estimate the p-value for the differences in mean HbT between the low- and high-heterogeneous tumors with and without *a priori* information.A paired Student t-test was employed to determine whether there was a significant difference between *a priori* and no *priori* data.A p-value of 0.05 or less was considered significant. Receiver operating characteristic (ROC) analysis was used to evaluate the potential of this method to distinguish low-heterogeneous tumors.

3. RESULTS AND DISCUSSION

A. Low Heterogeneity

Angiogenesis in the early stages of tumor growth forms a dense network of blood vessels to deliver nutrients to the tumor area. This dense network of blood vessels results in a highly perfusive and homogenous tumor. This can be seen in Fig 2(a) when the peak Gd-DTPA

enhancement in the tumor region is overlaid on the T1-weighted MR image of rats 1 and 5. The increase in blood supply also causes tumors in this stage to exhibit high uniform Gd-DTPA enhancement throughout the whole tumor. The tumor can be located on the DOT total hemoglobin maps with and without MRI anatomical *a priori* information due to the increased hemoglobin concentration from angiogenesis. The stand-alone DOT image correlates well with the tumor region obtained by the MRI. However, when the MRI guidance is utilized, the total blood concentration is uniformly distributed in the tumor region as the *a priori* information loosely groups all the pixels of the tumor region together but at the same time allows the reconstruction algorithm the freedom to update an individual pixel.

B. High Heterogeneity

As the cancer progresses, the tumor grows and evolves such that the original blood supply is not sufficient to continue its growth. The tumor can recruit new blood vessels to alleviate some of this deficiency and further its growth. However, this lack of nutrients can result in cell death and lead to areas of necrosis in the interior of the tumor. This results in a tumor with lower blood perfusion and higher heterogeneity. This can be seen from Fig 3(a) in the DCE-MRI overlay of rats 7 and 10. Unlike the highly uniform enhancement seen in Fig 2(a), the Gd-DTPA enhancement of the tumor is characterized by a high enhancement on the tumor boundary due to the tumor rim angiogenesis and spotted with high and low areas of enhancement in the interior of the tumor. This indicates that the tumor has outgrown the nutrition supply, and the tissue has undergone some necrosis. In the optical images, the tumor and muscle regions are indicated by the dashed black and green lines, respectively. Similar to the previous case, the DOT total hemoglobin maps with and without the MRI tumor boundary information correlates well with the tumor region from the MRI. However, unlike the DCE-MRI image, the optical images present high enhancement within the tumor, indicating that the stand-alone DOT lacks sufficient spatial resolution to reveal tumor heterogeneity.

C. Total Hemoglobin Concentration

The rats were split into two categories defined by their DCE-MRI Enhancement Fraction: low and high tumor heterogeneity.

Five animals were found to have low heterogeneous tumors with high perfusion, while the other five had low perfusion tumors with high heterogeneity. The tumor size also correlates with the heterogeneity as the early stages of the tumor are smaller and have a dense network of blood vessels which is indicated by the higher enhancement fraction. The recovered hemoglobin concentrations within the ROIs are calculated for all ten animals from the reconstructed DOT images both with and without MR anatomical *a priori* information. Table 1 shows the HbT values averaged over the tumor and muscle ROIs for these two groups along with their tumor size and enhancement fraction.

Without anatomical guidance, the stand-alone DOT shows a higher HbT of the tumor compared to muscle region due to the abundant vasculature in the tumor. However, it is unable to distinguish between the high and low heterogeneous tumors. As seen in Table 1,

the HbT for the DOT without MR *a priori* for the high and low heterogeneous tumors are nearly identical. The HbT is expected to be higher in the low heterogeneous tumors due to the higher vasculature of these early stage tumors. However, with the addition of the MR *a priori* information, there is a significant difference between the HbT for the high and low heterogeneous tumors. As the vasculature inside the muscle region is separate from the tumor, the HbT in the muscle is expected to be similar for both low and high heterogeneous tumor types. Thus, data in the muscle region serves as a control to determine the quality of the DCE-MRI and DOT measurements. Indeed, Table 1 shows that with the addition of the MR anatomical information, the recovered mean HbT in the muscle regions is slightly elevated but within the standard deviation and thus independent of the vascular heterogeneity in the tumor.

Figure 4 shows the mean and standard deviation for the HbT in the tumor and muscle ROI. Without MR guidance, the mean HbT for the low and high heterogeneous tumors are nearly identical at 133.7 ± 22.3 μM and 134.2 ± 32.6 μM, respectively. The muscle region showed similar mean HbTs of 76.2 ± 12.4 μM and 90.1.2 ± 23.0 μM for the low and high heterogeneous tumors, respectively, with the error bars overlapping.

On the other hand, with the addition of MR *a priori*, the difference between the low and high heterogeneous tumors becomes significant: 212.6 ± 44.1 μM and 150.7 ± 22.4 μM. Although there is a slight overlap with the standard deviations, a two-sample Student t-test found that they are statistically different with a p-value of 0.02. Meanwhile, the muscle region was similar to the no priori case, as there was no significant difference between the low and high heterogeneous tumors at 88.4 ± 28.8 μM and 109.4 ± 39.9 μM, respectively.

In addition, ROC analysis was performed to assess the ability to detect low heterogeneous tumors using the tumor mean HbT. These preliminary results using the HbT recovered with the addition of MR a priori showed much promise. The area under the curve (AUC) was found to be 0.88 with a sensitivity of 80% and specificity of 100%. In comparison, the HbT recovered without MR *a priori* showed a lower sensitivity (60%) and specificity (80%) with an AUC of 0.6. A limiting factor in the data analysis was the low number of rats used in this preliminary study.

Interestingly, a paired t-test comparing the mean HbT recovered with and without *a priori* showed that only the tumors with low heterogeneity showed a significant difference (p-value 0.016) between the two groups when the MRI *a priori* information was added, as seen in Table 2. With MR *a priori*, the mean HbT increased 58.9% for the tumors with low heterogeneity compared to only 12.3% for the tumors with high heterogeneity. The percent increase for the muscle when the *a priori* information was applied was similar at 25.9% and 21.4% for the low and high heterogeneous tumors, respectively. This follows as the T1-weighted MR image is used to define the tumor boundary, which is defined as one region in the DOT reconstruction FEM mesh. This anatomical information works well for the homogenous early stage tumors. However, when applied to the heterogeneous tumors, the anatomical ROI *a priori* information fails to provide an accurate guide for the hemoglobin concentration. Instead, a more accurate guide would be to use the functional information of the DCE-MRI's enhancement maps. However, it is interesting to note that this method is

able to separate the tumors with high and low heterogeneity without the use of the DCE-MRI and an exogenous contrast agent.

4. CONCLUSION

In summary, we present a method to differentiate between tumors with low and high heterogeneity tumors in vivo using MR-guided DOT without the use of an exogenous contrast agent and validated by a DCE-MRI. The results of our small scale animal study show that stand-alone DOT was able to localize the tumor, however, it was only with the addition of the *a priori* MR anatomical information that there was a significant difference between the two tumor stages. These preliminary results confirm that DOT alone lacks the resolution to resolve the heterogeneity of the tumor without the help of a higher resolution imaging modality and shows the potential of guided DOT for characterization of tumor heterogeneity. Although this particular hybrid MRI-DOT system is impractical for low cost screening and imaging, as only the tumor boundary is needed to provide structural *a priori* information, this shows that other imaging modalities such as an ultrasound, which is inexpensive and portable, has much more potential as seen in the study by Zhu *et al*. [44].

Unlike the study by Zhu *et al*. (2005) where they mapped the heterogeneous areas of tumor angiogenesis in large tumors that were confirmed to be necrotic, in this study, the tumors studied are in an earlier stage of growth (0.69–2.47 cm), and range from uniform tumor vasculature to more mature stages of tumor angiogenesis where the tumor has outgrown its blood supply and heterogeneous areas have developed. Previous research using DOT to measure the heterogeneity of tumor vasculature focuses heavily on human subjects for breast cancer, and there is a lack of animal systems and data [44]. To the best of our knowledge, this is the first in vivo animal study to non-invasively characterize and confirm different stages of tumor vascular heterogeneity using image-guided DOT and DCE-MRI, respectively. A DCE-MRI was performed in the same imaging session immediately following the DOT measurements to provide the highest degree of correlation and accuracy. Unlike the previous studies which required tissue sampling at various positions of the tumor to confirm vascular heterogeneity using histologic MVD counts, the uniqueness of this hybrid MRI-DOT system enables in vivo, noninvasive functional confirmation mere seconds after the DOT measurements without any movement or alteration of the system set up or animal other than the gadolinium injection [44]. Not only does this reduce the variables and errors that can occur when correlating different validation methods, but the fact that the DCE-MRI allows for a noninvasive confirmation of the DOT results holds much potential for longitudinal studies. Although the DCE-MRI is a well-known method to measure changes in tumor vascular heterogeneity and angiogenesis, the correlation between the image-guided DOT and biological stages needs to be expanded [51]. This system allows for a unique opportunity to correlate image-guided DOT with the biological stages of cancer and provide immediate confirmation using the DCE-MRI. As this in vivo technique and system is non-invasive and does not require surgical interference, frequent DOT measurements can be taken throughout the entirety of the disease.

This opens up a wide array of preclinical applications. Having insight into the vasculature of the tumor in small animals has the potential to impact many areas of cancer research such as

studying different cancer disease progressions, drug development and treatment strategies, and even clinical care with the use of mouse drug avatars to provide personalized treatment for human patients [52,53]. Indeed, diffuse optical small animal imaging *in vivo* has much potential for drug development in preclinical pharmaceutical research. As one of the hallmarks of cancer, angiogenesis is a key component to the growth and spread of all cancers [54]. Much effort has been spent on developing antiangiogenic drugs that inhibit angiogenesis to slow tumor growth. Since FDA approval of the first antiangiogenic drug in 2004, Bevacizumab, the number of antiangiogenic drugs has increased with many more drugs in clinical trials. In addition, in some cancers, studies have shown increased effectiveness of antiangiogenic drugs when combined with other therapies such as chemotherapy [1]. Consequently, methods to image and measure angiogenesis and the changes in the tumor vasculature have considerable importance not only for diagnosis and treatment, but in the development of new therapies.

The results of this preliminary investigation show the feasibility of this new method to differentiate tumor vascular heterogeneity. However, a major limitation includes the low number of animals used for this small scale animal study. Thus, future work will be to expand this study into a full scale investigation to validate this method. In addition, other criteria will be investigated further to see whether image-guided DOT can differentiate between multiple grades of tumor heterogeneity.

Acknowledgments

Funding. National Institutes of Health (NIH) (R21 EB013387, R21CA191389, R01EB008716, R21EB013387, R33CA120175, P30CA062203); Ruth L. Kirschstein National Research Service Award (F31CA171915–01A1); UCI Eugene Cota-Robles Fellowship.

REFERENCES

1. Siemann D, “The unique characteristics of tumor vasculature and preclinical evidence for its selective disruption by tumor-vascular disrupting agents,” Cancer Treat. Rev 37, 63–74 (2011). [PubMed: 20570444]
2. Jackson A, O’Connor JPB, Parker GJM, and Jayson GC, “Imaging tumor vascular heterogeneity and angiogenesis using dynamic contrast-enhanced magnetic resonance imaging,” Clin. Cancer Res 13, 3449–3459 (2007). [PubMed: 17575207]
3. Pickles MD, Manton DJ, Lowry M, and Turnbull LW, “Prognostic value of pre-treatment DCE-MRI parameters in predicting disease free and overall survival for breast cancer patients undergoing neoadjuvant chemotherapy,” Eur. J. Radiol 71, 498–505 (2009). [PubMed: 18572340]
4. O’Connor JPB, Jackson A, Parker GJM, and Jayson GC, “DCE-MRI biomarkers in the clinical evaluation of antiangiogenic and vascular disrupting agents,” Br. J. Cancer 96, 189–195 (2007). [PubMed: 17211479]
5. Alic L, van Vliet M, van Dijke CF, Eggermont AM, Veenland JF, and Niessen WJ, “Heterogeneity in DCE-MRI parametric maps: a biomarker for treatment response?” Phys. Med. Biol 56, 1601–1616 (2011). [PubMed: 21335648]
6. Hawighorst H, Knapstein PG, Knopp MV, Weikel W, Brix G, Zuna I, Schã SO, Essig M, Vaupel P, and van Kaick G, “Uterine cervical carcinoma: comparison of standard and pharmacokinetic analysis of time-intensity curves for assessment of tumor angiogen-esis and patient survival,” Cancer Res 58, 3598–3602 (1998). [PubMed: 9721867]
7. Gaustad J, Benjaminsen IC, Ruud EM, and Rofstad EK, “Dynamic contrast-enhanced magnetic resonance imaging of human melanoma xenografts with necrotic regions,” J. Magn. Reson. Imaging 26, 133–143 (2007). [PubMed: 17659570]

8. Brown JM and Giaccia AJ, “The unique physiology of solid tumors: opportunities (and problems) for cancer therapy,” Cancer Lett 58, 1408–1416 (1998).
9. O’Connor JPB, Jayson GC, Jackson A, Ghiorghiu D, Carrington BM, Rose CJ, Mills SJ, Swindell R, Roberts C, Mitchell CL, and Parker GJM, “Enhancing fraction predicts clinical outcome following first-line chemotherapy in patients with epithelial ovarian carcinoma,” Clin. Cancer Res 13, 6130–6135 (2007). [PubMed: 17947478]
10. Connor JPBO, Rose CJ, Jackson A, Watson Y, Cheung S, Maders F, Whitcher BJ, Roberts C, Buonaccorsi GA, Thompson G, Clamp AR, Jayson GC, and Parker GJM, “DCE-MRI biomarkers of tumour heterogeneity predict CRC liver metastasis shrinkage following bevacizumab and FOLFOX-6,” Brit. J. Cancer 105, 139–145 (2011). [PubMed: 21673686]
11. Boas D, Brooks DH, Miller EL, DiMarzio CA, Kilmer M, Gaudette RJ, and Zhang Q, “Imaging the body with diffuse optical tomography,” IEEE Signal Proc. Mag 18(6), 57–75 (2001).
12. Cerussi A, Shah N, Hsiang D, Durkin A, Butler J, and Tromberg BJ, “In vivo absorption, scattering, and physiologic properties of 58 maignant breast tumors determined by broadband diffuse optical spectroscopy,” J. Biomed. Opt 11, 044005 (2015).
13. Choe R, Konecky SD, Corlu A, Lee K, Durduran T, Busch DR, Pathak S, Czerniecki BJ, Tchou J, Fraker DL, DeMichele A, Chance B, Arridge SR, Schweiger M, Culver JP, Schnall MD, Putt ME, Rosen MA, and Yodh AG, “Differentiation of benign and malignant breast tumors by in vivo three-dimensional parallel-plate diffuse optical tomography,” J. Biomed. Opt 14, 024020 (2009). [PubMed: 19405750]
14. Pakalniskis MG, Wells WA, Schwab MC, Froehlich HM, Tosteson TD, Poplack SP, Kaufman PA, Pogue BW, and Paulsen KD, “Tumor angiogenesis change estimated by using diffuse optical spectroscopic tomography: demonstrated correlation in women undergoing neoadjuvant chemotherapy for invasive breast cancer?” Radiology 259, 365–374 (2011). [PubMed: 21406632]
15. Pogue BW, Poplack SP, McBride TO, Wells WA, Osterman KS, Osterberg UL, and Paulsen KD, “Quantitative hemoglobin tomography with diffuse near-infrared spectroscopy: pilot results in the breast,” Radiology 218, 261–266 (2001). [PubMed: 11152812]
16. Ntziachristos V, Yodh AG, Schnall M, and Chance B, “Concurrent MRI and diffuse optical tomography of breast after indocyanine green enhancement,” Proc. Natl. Acad. Sci. USA 97, 2767–2772 (2000). [PubMed: 10706610]
17. Choe R, Corlu A, Lee K, Durduran T, Konecky SD, Grosicka-Koptyra M, Arridge SR, Czerniecki BJ, Fraker DL, DeMichele A, Chance B, Rosen MA, and Yodh AG, “Diffuse optical tomography of breast cancer during neoadjuvant chemotherapy: a case study with comparison to MRI,” Med. Phys 32, 1128–1139 (2005). [PubMed: 15895597]
18. Falou O, Soliman H, Sadeghi-Naini A, Iradji S, Lemon-Wong S, Zubovits J, Spayne J, Dent R, Trudeau M, Boileau JF, Wright FC, Yaffe MJ, and Czarnota GJ, “Diffuse optical spectroscopy evaluation of treatment response in women with locally advanced breast cancer receiving,” Transl. Oncol 5, 238–246 (2012). [PubMed: 22937175]
19. Choyke PL, Dwyer AJ, and Knopp MV, “Functional tumor imaging with dynamic contrast-enhanced magnetic resonance imaging,”J. Magn. Reson. Imaging 17, 509–520 (2003). [PubMed: 12720260]
20. Kotz KT, Dixit SS, Gibbs AD, Orduna JM, Haroon Z, Amin K, and Faris GW, “Inspiratory contrast for in vivo optical imaging,” Opt. Express 16, 19–31 (2008). [PubMed: 18521129]
21. Lin Y, Thayer D, Nalcioglu O, and Gulsen G, “Tumor characterization in small animals using magnetic resonance-guided dynamic contrast enhanced diffuse optical tomography,” J. Biomed. Opt 16, 106015 (2011). [PubMed: 22029362]
22. Dehghani H, Pogue BW, Shudong J, Brooksby B, and Paulsen KD, “Three-dimensional optical tomography: resolution in small-object imaging,” Appl. Opt 42, 3117–3128 (2003). [PubMed: 12790463]
23. Pogue BW, Davis SC, Leblond F, Mastanduno M, Dehghani H, and Paulsen KD, “Implicit and explicit prior information in near-infrared spectral imaging: accuracy, quantification and diagnostic value,” Philos. Trans. R. Soc. A 369, 4531–4557 (2011).
24. Hielscher AH, “Optical tomographic imaging of small animals,” Curr. Opin. Biotechnol 16, 79–88 (2005). [PubMed: 15722019]

25. Fang Q, Selb J, Carp SA, Boverman G, Miller EL, Brooks DH, Moore RH, Kopans DB, and Boas DA, “Combined optical and x-ray tomosynthesis breast imaging,” Radiology 258, 89–97 (2011). [PubMed: 21062924]
26. Biswal N, Xu Y, and Zhu Q, “Imaging tumor oxyhemoglobin and de- oxyhemoglobin concentrations with ultrasound-guided diffuse optical tomography,” Technol. Cancer Res. Treat 10, 417–429 (2011). [PubMed: 21895027]
27. Brooksby B, Pogue BW, Jiang S, Dehghani H, Srinivasan S, Kogel C, Tosteson TD, Weaver J, Poplack SP, and Paulsen KD, “Imaging breast adipose and fibroglandular tissue molecular signatures by using hybrid MRI-guided near-infrared spectral tomography,” Proc. Natl. Acad. Sci. USA 103, 8828–8833 (2006). [PubMed: 16731633]
28. Zhu Q, Huang M, Chen N, Zarfos K, Jagjivan B, Kane M, Hedge P, and Kurtzman SH, “Ultrasound-guided optical tomographic imaging of malignant and benign breast lesions: initial clinical results of 19 cases,” Neoplasia 5, 379–388 (2003). [PubMed: 14670175]
29. Ale A, Ermolayev V, Herzog E, Cohrs C, de Angelis MH, and Ntziachristos V, “FMT-XCT: in vivo animal studies with hybrid fluorescence molecular tomography-x-ray computed tomography,” Nat. Methods 9, 615–620 (2012). [PubMed: 22561987]
30. Darne CD, Lu Y, Tan I-C, Zhu B, Rasmussen JC, Smith AM, Yan S, and Sevick-Muraca EM, “A compact frequency-domain photon migration system for integration into commercial hybrid small animal imaging scanners for fluorescence tomography,” Phys. Med. Biol 57, 8135–8152 (2012). [PubMed: 23171509]
31. Davis SC, Pogue BW, Springett R, Leussler C, Mazurkewitz P,Tuttle SB, Gibbs-Strauss SL, Jiang SS, Dehghani H, and Paulsen KD, “Magnetic resonance-coupled fluorescence tomography scanner for molecular imaging of tissue,” Rev. Sci. Instrum 79, 064302 (2008). [PubMed: 18601421]
32. Xu JH, Springett R, Dehghani H, Pogue BW, Paulsen KD, and Dunn F, “Magnetic-resonance-imaging-coupled broadband near-infrared tomography system for small animal brain studies,” Appl. Opt 44, 2177–2188 (2005). [PubMed: 15835363]
33. Klose AD, Beattie BJ, Dehghani H, Vider L, Le C, Ponomarev V, and Blasberg R, “In vivo bioluminescence tomography with a blocking-off finite-difference SP3 method and MRI/CT coregistration,” Med. Phys 37, 329–338 (2010). [PubMed: 20175496]
34. Guggenheim JA, Basevi HRA, Frampton J, Styles IB, and Dehghani H, “Multi-modal molecular diffuse optical tomography system for small animal imaging,” Meas. Sci. Technol 24, 105405 (2013). [PubMed: 24954977]
35. Lin Y, Ghijsen M, Nalcioglu O, and Gulsen G, “In vivo validation of quantitative frequency domain fluorescence tomography,” J. Biomed. Opt 17, 126021 (2012). [PubMed: 23323291]
36. Venugopal V, Chen J, Lesage F, and Intes X, “Full-field time-resolved fluorescence tomography of small animals,” Opt. Lett 35, 3189–3191 (2010). [PubMed: 20890329]
37. Zhang Y, Zhang B, Liu F, Luo J, and Bai J, “*In vivo* tomographic imaging with fluorescence and MRI using tumor-targeted dual-labeled nanoparticles,” Int. J. Nanomed 9, 33–41 (2014).
38. Li C, Yang Y, Mitchell GS, and Cherry SR, “Simultaneous PET and multispectral 3-dimensional fluorescence optical tomography imaging system,” J. Nucl. Med 52, 1268–1275 (2011). [PubMed: 21810591]
39. Solomon M, Nothdruft RE, Akers W, Edwards WB, Liang K, Xu B, Suddlow GP, Deghani H, Tai Y-C, Eggebrecht AT, Achilefu S, and Culver JP, “Multimodal fluorescence-mediated tomography and SPECT/CT for small-animal imaging,” J. Nucl. Med 54, 639–646 (2013). [PubMed: 23447655]
40. Liu S, Zhang B, Wang X, Li L, Chen Y, Liu X, Liu F, Shan B, and Bai J, “A dual modality system for simultaneous fluorescence and positron emission tomography imaging of small animals,” IEEE Trans. Nucl. Sci 58, 51–57 (2011).
41. Lu Y, Machado HB, Bao Q, Stout D, Herschman H, and Chatziioannou AF, “In vivo mouse bioluminescence tomography with radionuclide-based imaging validation,” Mol. Imaging Biol 13, 53–58 (2011). [PubMed: 20464517]
42. Flexman ML, Vlachos F, Kim HK, Sirsi SR, Huang J, Hernandez SL, Johung TB, Gander JW, Reichstein AR, Lampl BS, Wang A, Borden MA, Yamashiro DJ, Kandel JJ, and Hielscher AH,

"Monitoring early tumor response to drug therapy with diffuse optical tomography," J. Biomed. Opt 17, 016014 (2012). [PubMed: 22352664]

43. Gibson AP, Hebden JC, and Arridge SR, "Recent advances in diffuse optical imaging," Phys. Med. Biol 50, R1–R43 (2005). [PubMed: 15773619]
44. Zhu Q, Kurtzma SH, Hegde P, Tannenbaum S, Kane M, Huang M, Chen NG, Jagjivan B, and Zarfos K, "Utilizing optical tomography with ultrasound localization to image heterogeneous hemoglobin distribution in large breast cancers," Neoplasia 7, 263–270 (2005). [PubMed: 15799826]
45. Gulsen G, Birgul O, Burcin Unlu M, Shafiiha R, and Nalcioglu O, "Combined diffuse optical tomography (DOT) and MRI system for cancer imaging in small animals," Technol. Cancer Res. Treat 5, 351–363 (2006). [PubMed: 16866566]
46. Robinson SP, McIntyre DJO, Checkley D, Tessier JJ, Howe FA, Griffiths JR, Ashton SE, Ryan AJ, Blakey DC, and Waterton JC, "Tumour dose response to the antivascular agent ZD6126 assessed by magnetic resonance imaging," Br. J. Cancer 88, 1592–1597 (2003). [PubMed: 12771928]
47. Yalavarthy PK, Pogue BW, Dehghani H, Carpenter CM, Jiang S, and Paulsen KD, "Structural information within regularization matrices improves near infrared diffuse optical tomography," Opt. Express 15, 8043–8058 (2007). [PubMed: 19547132]
48. Haskell RC, Svaasand LO, Tsay TT, Feng TC, McAdams MS, and Tromberg BJ, "Boundary conditions for the diffusion equation in radiative transfer," J. Opt. Soc. Am. A 11, 2727–2741 (1994).
49. S. R. Arridge, "Optical tomography in medical imaging," Inverse Probl 15, R41–R93 (1999).
50. Ghijsen M, Lin Y, Hsing M, Nalcioglu O, and Gulsen G, "Optimal analysis method for dynamic contrast-enhanced diffuse optical tomography," Int. J. Biomed. Imaging 2011, 1–13 (2011).
51. Perini R, Choe R, Yodh AG, Sehgal C, Divgi CR, and Rosen MA, "Non-invasive assessment of tumor neovasculature: techniques and clinical applications," Cancer Metastasis Rev 27, 615–630 (2008). [PubMed: 18506398]
52. Malaney P, Nicosia SV, and Davé V, "One mouse, one patient paradigm: new avatars of personalized cancer therapy," Cancer Lett 344, 1–12 (2014). [PubMed: 24157811]
53. Garralda E, Paz K, López-Casas PP, Jones S, Katz A, Kann LM, López-Rios F, Sarno F, Al-Shahrour F, Vasquez D, Bruckheimer E, Angiuoli SV, Calles A, Diaz LA, Velculescu VE, Valencia A, Sidransky D, and Hidalgo M, "Integrated next-generation sequencing and avatar mouse models for personal-ized cancer treatment," Clin. Cancer Res 20, 2476–2484 (2014). [PubMed: 24634382]
54. Hanahan D and Weinberg RA, "Hallmarks of cancer: the next generation," Cell 144, 646–674 (2011). [PubMed: 21376230]

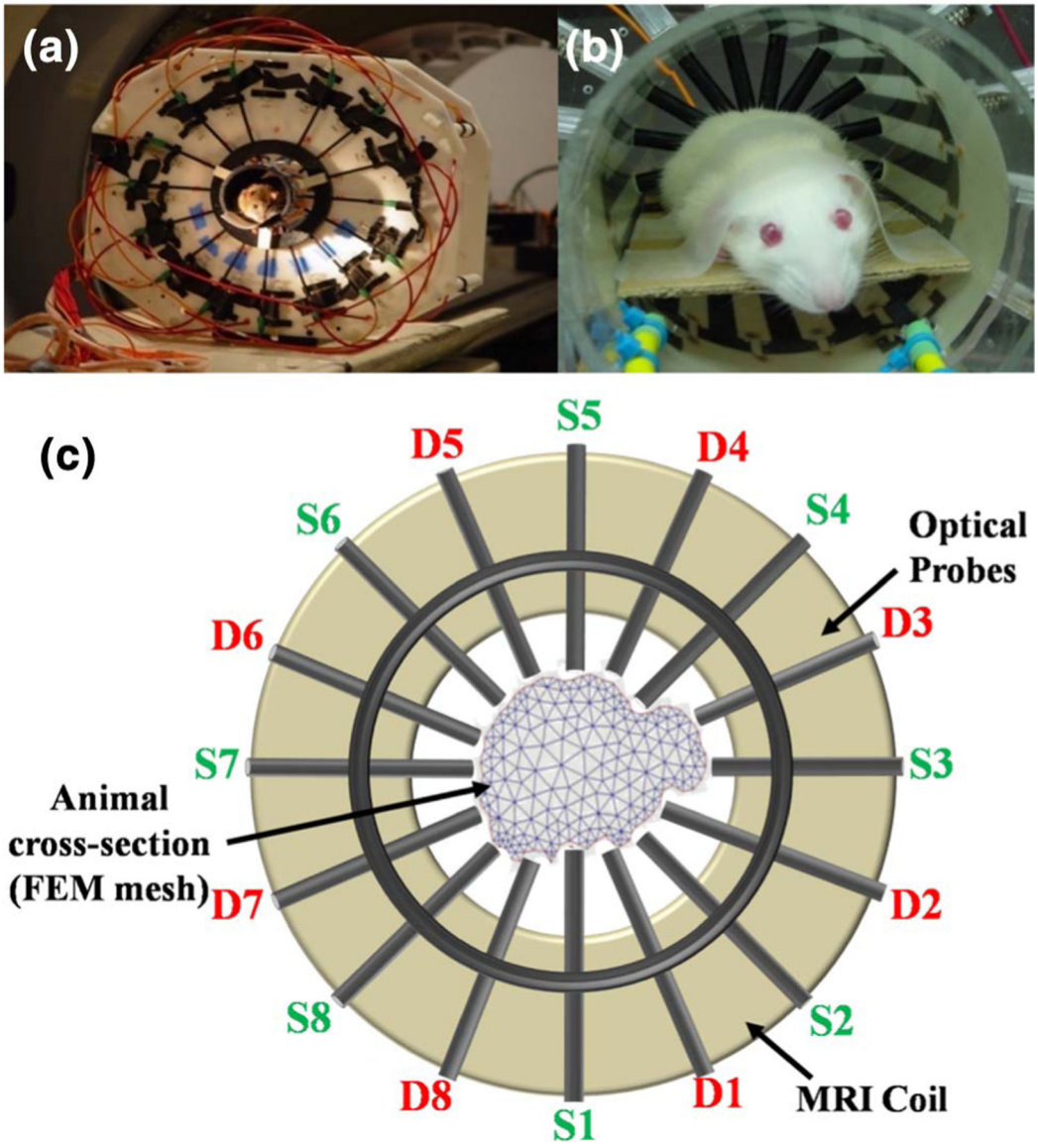

Fig. 1.

(a) Hybrid multi-wavelength MRI-DOT system animal holder and interface. (b) Close up of animal holder. (c) Schematic of interface. A 16-leg birdcage RF-coil is integrated into the interface to be able to acquire both optical and MRI measurements simultaneously. There are eight detectors and eight sources in a radial pattern, and each probe is adjusted until it comes in contact with the skin.

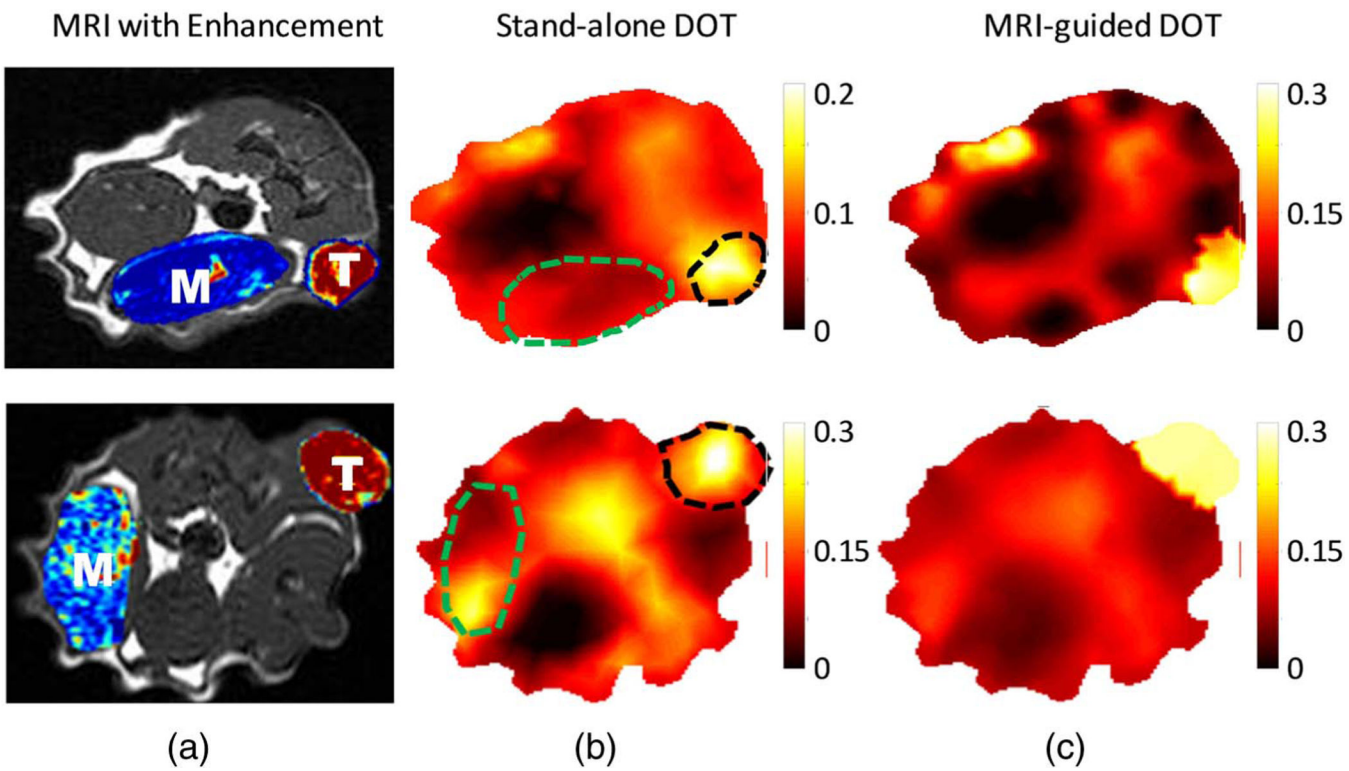

Fig. 2.

Low heterogeneous tumors with strong uniform enhancement in the tumor. The images in the top and bottom row correspond to rat 1 and 5, respectively, in Table 1. (a) T1 weighted MR images of the rat with the peak DCE enhancement map of the tumor (indicated as “T”) and muscle (indicated as “M”) region superimposed. The DOT reconstructed HbT maps (μM) (b) without and (c) with MRI structural a priori information is shown. The T and M region are indicated by black and green dashed lines.

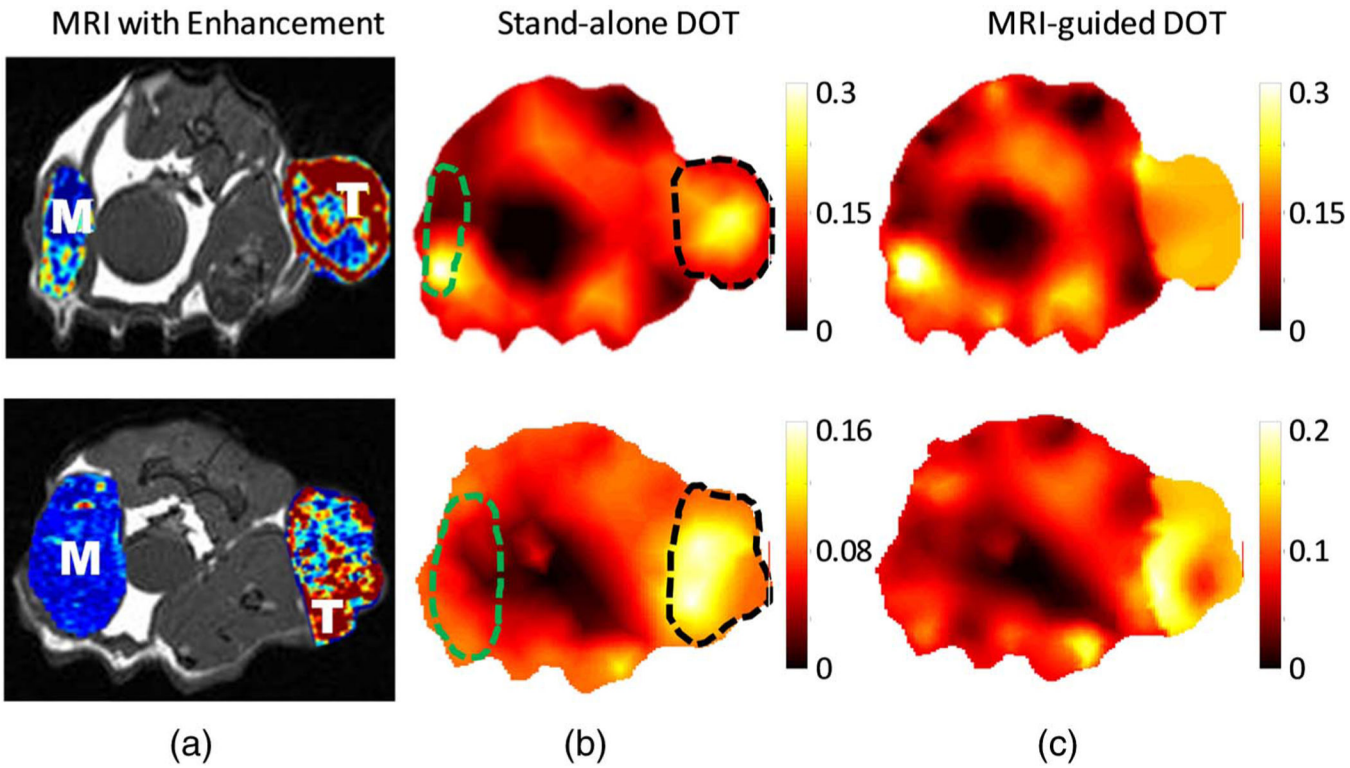

Fig. 3.

High heterogeneous tumors with irregular enhancement in the tumor. The images in the top and bottom row correspond to rat 7 and 10, respectively, in Table 1. (a) T1 weighted MR images of the rat with the peak DCE enhancement map of the tumor (indicated as “T”) and muscle (indicated as “M”) region superimposed. The DOT reconstructed HbT maps (μM) (b) without and (c) with MRI structural a priori information is shown. The T and M region are indicated by black and green dashed lines.

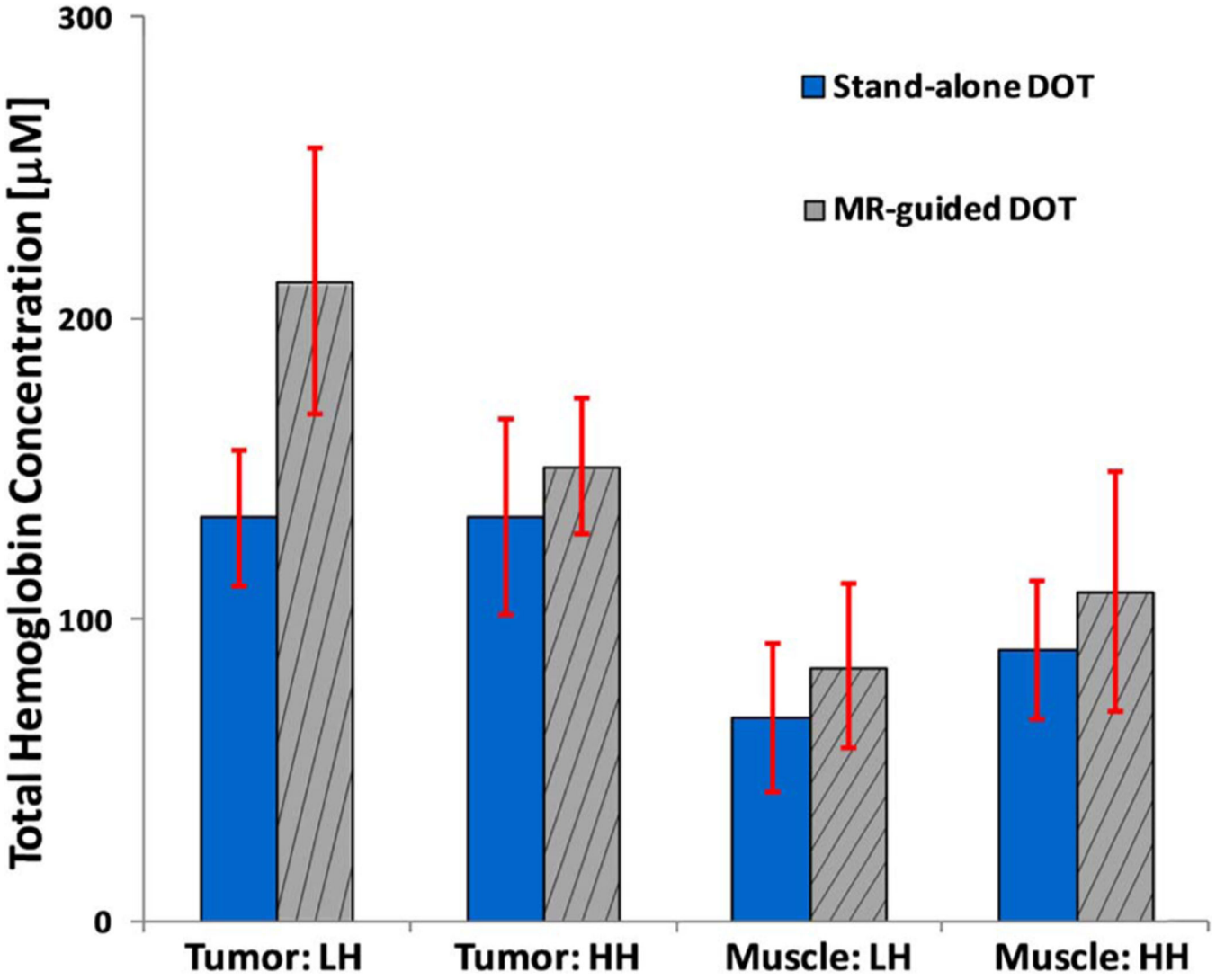

Fig. 4.

Averaged HbT (μM) for both tumor and muscle regions recovered using stand-alone DOT (solid) with no *priori* information and a MR-guided DOT (striped) with the *a priori* information. The low and high heterogeneous cases are abbreviated as LH and HH, respectively. The standard deviations are also given.

Table 1.

Summary of Tumor Stages for 10 Animals[a]

			Tumor: Mean HbT (μM)		Muscle: Mean HbT (μM)	
Rat No.	**Heterogeneity Level**	**Tumor Size (cm)**	**No APR**	**APR**	**No APR**	**APR**
1	Low	1	137.8	255.4	77.9	80.6
2	Low	0.98	168.4	237.8	73.2	130
3	Low	0.69	107.6	237.5	72.2	104.5
4	Low	1.68	130.1	179.7	95.7	67.1
5	Low	1.34	124.8	152.4	61.9	60
Mean			133.7±22.3	212.6±44.1	76.2±12.4	88.4±28.8
6	High	2.06	133.1	179.1	68.7	75
7	High	2.37	106.1	160.2	97.3	92.2
8	High	2.13	118.2	158.4	91.7	115
9	High	1.91	189.9	127.8	124	176
10	High	2.47	123.5	127.8	68.7	88.6
Mean			134.2±32.7	150.7±22.4	90.1±23.0	109.4±39.9

[a]The recovered mean total hemoglobin concentration (HbT) at both tumor and muscle regions for each animal are shown without and with MR *a priori* (APR). The units of HbT is micromolar (μM) and the unit for tumor size is centimeter (cm). The tumors were classified as low or high heterogeneity based on the enhancement fraction (EF). The mean values and standard deviations for both groups are also provided.

Table 2.

Paired t-test for Mean Difference in Averaged Total Hemoglobin Concentration with and without MR *a priori* Information

	Tumor		Muscle	
Heterogeneity	**Low**	**High**	**Low**	**High**
P-value	0.016[a]	0.484	0.452	0.116

[a]Significant.